

PCCP

Accepted Manuscript



This is an *Accepted Manuscript*, which has been through the Royal Society of Chemistry peer review process and has been accepted for publication.

Accepted Manuscripts are published online shortly after acceptance, before technical editing, formatting and proof reading. Using this free service, authors can make their results available to the community, in citable form, before we publish the edited article. We will replace this *Accepted Manuscript* with the edited and formatted *Advance Article* as soon as it is available.

You can find more information about *Accepted Manuscripts* in the [Information for Authors](#).

Please note that technical editing may introduce minor changes to the text and/or graphics, which may alter content. The journal's standard [Terms & Conditions](#) and the [Ethical guidelines](#) still apply. In no event shall the Royal Society of Chemistry be held responsible for any errors or omissions in this *Accepted Manuscript* or any consequences arising from the use of any information it contains.

Cite this: *Phys. Chem. Chem. Phys.*, 2015, XX,

www.rsc.org/xxxxxx

PAPER

Preparation of Ni@C/Cd_{0.8}Zn_{0.2}S nanocomposite with highly efficient and stable photocatalytic hydrogen production activity

Jinyan Liu, Chuansheng Zhuang, Kan Li and Tianyou Peng*

Received Xth XXXX 20XX, Accepted Xth XXXX 20XX

DOI: 10.1039/c1cp000000x.

A series of carbon-coated Ni (Ni@C)/Cd_{0.8}Zn_{0.2}S nanocomposite was fabricated *via* a facile hydrothermal process by using a pre-prepared Ni@C as starting material. The obtained products were characterized by X-ray diffraction, UV-vis diffuse reflectance absorption spectrum, X-ray photoelectron spectroscopy and electron microscopy. It is found that the introduction of Ni@C nanoparticles can improve both the visible-light-induced photocatalytic H₂ production activity and stability of the Cd_{0.8}Zn_{0.2}S solid solution, and the Ni nanoparticles encapsulated by several graphite-like carbon layers show a high chemical and thermal stability. Among those products with various Ni@C contents, 5wt% Ni@C/Cd_{0.8}Zn_{0.2}S nanocomposite exhibits the maximum photoactivity (969.5 μmol h⁻¹) for H₂ production, which is ~3.10 times higher than that (312.6 μmol h⁻¹) of the pristine Cd_{0.8}Zn_{0.2}S. This significant enhancement in the photoactivity by loading Ni@C nanoparticles can be attributed to the metallic Ni in Ni@C acted as co-catalyst while the graphite-like carbon shells as Cd_{0.8}Zn_{0.2}S nanoparticles' support and electron acceptor, which causing an effective photogenerated carrier separation in space and the improvement of the photoactivity and stability for H₂ production. The present findings demonstrate a cost reduction strategy by using non-noble metal co-catalyst for efficient and stable light-to-hydrogen energy conversion.

1. Introduction

Since the pioneering work on the photoelectrochemical splitting of water into H₂ and O₂ over TiO₂ electrode was first reported in 1972,¹ photocatalytic H₂ production over semiconductor is considered as one of the promising solutions to the growing crisis in energy due to its potential application in the clean hydrogen energy production from water by utilizing the inexhaustible solar energy.²⁻⁷ As a visible-light-induced photocatalyst, CdS loading with Pt as co-catalyst has been extensively studied because of its excellent photoactivity for H₂ production, in that its bandgap (~2.42 eV) corresponds well with the solar spectrum and its conduction band (CB) edge is more negative than the H₂O/H₂ redox potential for the water reduction.⁸⁻¹⁰ Nevertheless, those metal sulphides especially for CdS are prone to photocorrosion during the photoreaction process, where metal sulphide is itself oxidized by the photogenerated holes, which retards its large-scale application.¹¹ Therefore, many strategies have been developed to improve the photoactivity and stability of metal sulphide photocatalysts, for instance, by loading the noble metal, changing the preparation process and/or introducing the sulphide into the layered or porous inorganic substances.¹²⁻¹⁴

Incorporation of ZnS into CdS to form Cd_xZn_{1-x}S (0<x<1) solid solution has been proved to be an effective approach to

improve the photoactivity of CdS since the more negative CB edge of ZnS has a stronger ability to reduce water for H₂ production though its bandgap is wider than CdS.^{4,15-17} Also, Zn²⁺ with ion radius (0.74 Å) smaller than Cd²⁺ (0.97 Å) can supply stronger connection among atoms in the solid solution, causing an improved photostability of CdS.^{16,18} Namely, the formation of Cd_{1-x}Zn_xS solid solution can improve both photoactivity and stability of CdS, especially for the photocatalytic H₂ production in the absence of noble metal co-catalyst.¹⁵⁻¹⁹ Moreover, the energy band structure and the visible-light-induced activity of the Cd_{1-x}Zn_xS solid solutions can be conveniently tuned by adjusting the x value, and the Cd_{0.8}Zn_{0.2}S solid solution with Cd/Zn atom molar ratio of ~4 seems to show the maximum activity for H₂ production among various Cd_{1-x}Zn_xS solid solutions.^{15,19}

On the other hand, noble metals such as Pt, Pd, and Rh are generally loaded on CdS nanoparticles as co-catalyst to provide active sites for the photoreaction and suppress the charge recombination.¹⁵⁻¹⁹ In view of the practical application, cost reduction of the photocatalytic H₂ production system is one of the key issues. Thus, some non-noble metals such as Cu, Ni and/or their oxides have been investigated as alternative to those noble metals for promoting the photogenerated carrier separation and acting as water reduction sites.²⁰⁻²² However, the chemical stability and photoactivity of the prepared products are far from being satisfactory for its practical application,²⁰⁻²² and thus the development of photocatalysts with high visible-light-induced

College of Chemistry and Molecular Science, Wuhan University, Wuhan 430072, China. E-mail: typeng@whu.edu.cn (T.Y. Peng).

activity and stability for cheap and efficient light-to-hydrogen energy conversion is currently an intensive research topic.²¹⁻²⁵

The above drawbacks of co-catalysts might be overcome by metal encapsulation strategy with metal oxide or even carbon shell, which shows excellently chemical and thermal stability.²⁶⁻²⁸ An important progress in this direction is core-shell-structured co-catalyst, consisting of a noble metal (Rh, Pd and Pt) or metal oxide (NiO_x, RuO₂ and Rh₂O₃) core and a chromia (Cr₂O₃) shell, which resulted in enhanced visible-light-induced activity for H₂ production over GaN/ZnO due to the suppression of undesirable reverse reactions (H₂-O₂ recombination) and/or protection of the core component from chemical corrosion depending on the core type.²⁸ Recently, an integrated strategy was employed to prepare visible-light-induced semiconducting metal oxide or sulphide nanocomposites by incorporating carbon-coated Ni (Ni@C) nanoparticles as co-catalyst in our group, it was found that the obtained nanocomposites exhibited considerable stability and photoactivity for H₂ production,^{29,30} and the carbon encapsulation strategy can not only utilize the metallic Ni in Ni@C as co-catalyst but also the graphite-like carbon coating as semiconductor nanoparticles' support and electron acceptor, and consequently leading to the efficient charge separation and high stability both for sulphide and metallic Ni co-catalyst.³⁰

Herein, Cd_{0.8}Zn_{0.2}S was selected for the subject of the photocatalyst because this solid solution with Cd/Zn atomic ratio of 4 has the maximum photoactivity for H₂ production according to the previous reports,^{4,15} and a series of Ni@C/Cd_{0.8}Zn_{0.2}S nanocomposites with different Ni@C contents was prepared *via* a facile hydrothermal process by using a pre-prepared Ni@C as starting material. The effects of Ni@C content in the Ni@C/Cd_{0.8}Zn_{0.2}S on the crystal structure, spectral absorption, stability and photoactivity for H₂ production under visible light were investigated in detail. A significantly enhanced visible-light-induced photoactivity and stability for H₂ production as compared to the pristine Cd_{0.8}Zn_{0.2}S are both achieved in the present study.

2. Experimental

2.1 Material preparation

All chemical reagents used were obtained from commercial sources as guaranteed-graded reagents and used without further purification. Ni@C nanoparticles were prepared by an AC arc discharge method under He gas atmosphere according to the previous publication.³¹ Before using for the material preparation, 2.0 M HCl solution was used to treat the Ni@C nanoparticles to remove the uncoated metallic Ni particles.^{29,30} The as-prepared Ni@C product has particle size distribution in the range of 10-50 nm, and contains 67.54wt% face-centred cubic (FCC) Ni nanocrystals encapsulated by graphite-like carbon shells.³¹

Ni@C/Cd_{0.8}Zn_{0.2}S was prepared by a facile hydrothermal process similar to the previous work but with some modification.⁴ Typically, 0.213 g Cd(Ac)₂·2H₂O, 0.051 g ZnAc₂·2H₂O, 7.8 mg Ni@C, and 1.44 g sodium dodecyl sulfonate (SDS) were added in 50 mL water under stirring. After sonication for 15 min, 0.150 g thioacetamide (TAA) was added into the suspension, and then transferred into a Teflon-lined stainless steel autoclave from hydrothermal treatment at 100 °C for 3 h. The obtained sample was washed with acetone and alcohol in sonication washer to

remove non-reacted reactants, and then dried at 60 °C overnight to obtain 5wt% Ni@C/Cd_{0.8}Zn_{0.2}S.

For comparison, Ni@C/Cd_{0.8}Zn_{0.2}S nanocomposites with different Ni@C contents were prepared by varying the Ni@C addition amount. The pristine Cd_{0.8}Zn_{0.2}S was also prepared via the same process but without addition of Ni@C. Pt-loading of Cd_{0.8}Zn_{0.2}S was conducted according to a typical photodeposition method. 0.2 g Cd_{0.8}Zn_{0.2}S was dispersed into 40 mL water under stirring, and then 10 mL methanol and 0.65 mL H₂PtCl₆ (0.077 M) solution were added in the suspension in sequence. The mixture was irradiated by a 500 W high-pressure Hg-lamp for 3 h under stirring. After centrifugation, the sample was washed with water and dried at 80 °C for 10 h to obtain 5wt% Pt/Cd_{0.8}Zn_{0.2}S.

2.2 Material characterization

X-ray powder diffraction (XRD) patterns were obtained on a Bruker D8 advance X-ray diffractometer with Cu K α radiation (λ = 0.15418 nm). Product morphology was observed on JEOL JEM 2100F high-resolution transmission electron microscope (HRTEM) working at 200 kV. X-ray photoelectron spectra (XPS) were recorded on a Kratos XSAM800 X-ray photoelectron spectroscope equipped with a standard and monochromatic source (Al K α). The diffuse reflectance absorption spectra (DRS) were recorded on a Cary 5000 UV-Vis-NIR spectrophotometer equipped an integrating sphere by using BaSO₄ as a reference. Photoluminescence (PL) spectra were obtained on a Hitachi F4500 fluorometer. The contents of various elements in sample were detected by using Bruker S4 Pioneer X-ray fluorescence (XRF) spectrometer with Rh target without standard sample.

For the photoelectrochemical measurement, a working electrode (Pt wire) was immersed in a 50 mL of suspension containing photocatalyst (25 mg), NaOH (1.9 g) and methyl viologen (6 mg), and a saturated Ag/AgCl electrode and a Pt gauze electrode were used as a reference and a counter electrode, respectively. Before irradiation, the suspension was continuously purged by N₂ to remove O₂, and then illuminated by visible light ($\lambda \geq 420$ nm) from a 300W Xe-lamp equipped with a 420 nm cutoff filter. The working electrode was held at +0.4 V *vs.* Ag/AgCl, and the photocurrent-time curve was collected by using a CHI618 workstation.⁷ To evaluate the photostability, the photocatalyst after the first run of 5 h photochemical reaction was picked out from the suspension, washed with water and dried at 70 °C. And then this recovered photocatalyst was used to the second run of the photoreaction under the same condition. The Cd²⁺ and Ni²⁺ in the remnant solutions after each run photoreaction and removal of the photocatalyst were collected by a 731 positive ion-exchange resin and, their concentrations were detected by a WFX-200 atomic absorption spectrometer (AAS, Beijing Rayleigh Analytical Instrument Co. Ltd. China) with Deuterium Lamp effect background correction system.

2.3 Photoactivity measurement

Photocatalytic H₂ evolution reactions were carried out in an outer irradiation-type photoreactor (pyrex glass). The photocatalyst (0.10 g) was dispersed in 100 mL sacrificial reagent solution containing 0.25 M Na₂SO₃ and 0.35 M Na₂S aqueous solution, which can serve as hole scavengers and allow an effectual H₂ production. A 300 W Xe-lamp (PLS-SXE300, Beijing Trusttech Co. Ltd, China) with a cutoff filter (Kenko L-42) was employed

for visible-light ($\lambda \geq 420$ nm) irradiation. Before the light irradiation, the photoreactor containing photocatalyst and the sacrificial reagent was sonicated several minutes to let the photocatalyst dispersed uniformly, and then thoroughly degassed to remove air completely. The H_2 evolved amount was determined by a gas chromatograph (GC, SP-6800A, TCD, 5 Å molecular sieve columns and Ar carrier).

Apparent quantum yield (AQY) was measured under the same photoreaction condition except for the incident monochromatic light.^{4,7} The H_2 yields of 1 h photoreaction under different monochromatic light wavelengths were measured. The band-pass and cutoff filters and a calibrated Si photodiode (SRC-1000-TC-QZ-N, Oriel, USA) were used in the above measurement. The AQY values at different monochromatic light wavelengths were calculated by the following equation.^{4,7}

$$\text{AQY (\%)} = \frac{\text{The number of reacted electrons}}{\text{The number of incident photons}} \times 100$$

$$= \frac{2 \times \text{The number of evolved } H_2 \text{ molecules}}{\text{The number of incident photons}} \times 100$$

3. Results and discussion

3.1 Crystal phase and microstructure analyses

Fig. 1 depicts the XRD patterns of the pristine $Cd_{0.8}Zn_{0.2}S$ and $Ni@C/Cd_{0.8}Zn_{0.2}S$ nanocomposites with different Ni@C contents. As can be seen, the pristine $Cd_{0.8}Zn_{0.2}S$ shows three main diffraction peaks with 2θ located at *ca.* 26.6°, 44.2° and 52.4°, which is very similar to the three diffraction peaks at $2\theta=25.5^\circ$, 44° and 52°, ascribable to the (111), (220) and (311) planes of cubic CdS (JCPDS No. 42-1411).^{14,30} It indicates that CdS-ZnS solid solution (JCPDS No. 49-1302) is formed by the present hydrothermal process.^{4,21} The pristine Ni@C nanoparticles show a diffraction peak, basically consistent to the graphite's (002) planes diffraction peak with $2\theta \sim 26.5^\circ$ and the interlayer distance of 0.334 nm, indicating the carbon in Ni@C existed as graphite-like structures.^{29,30} Moreover, there are two obvious diffraction peaks with 2θ located at $\sim 44.6^\circ$ and $\sim 51.8^\circ$, ascribable to the (111) and (200) planes of face-centered cubic (FCC) Ni, indicating Ni in Ni@C existed as metallic nanoparticles even through the acid pretreated process.^{29,31}

All Ni@C/ $Cd_{0.8}Zn_{0.2}S$ nanocomposites with different Ni@C contents show obvious reflection peaks with 2θ located at *ca.* 26.6°, 44.2° and 52.4°, which is similar to the pristine $Cd_{0.8}Zn_{0.2}S$ (Fig. 1). It means that the $Cd_{0.8}Zn_{0.2}S$ in Ni@C/ $Cd_{0.8}Zn_{0.2}S$ also exists as cubic phase. The reflection peaks of Ni@C cannot obviously be observed from the XRD patterns of Ni@C/ $Cd_{0.8}Zn_{0.2}S$ with Ni@C content less than 5wt%, which might be due to its low content and high dispersion.^{12,20} Although these reflection peaks of Ni@C partly overlap with that of $Cd_{0.8}Zn_{0.2}S$ as shown in Fig. 1, the product with 9wt% Ni@C content shows a diffraction peak at $2\theta \sim 44.6^\circ$ attributable to the (111) planes of FCC metallic Ni (labelled by the dot line in Fig. 1), indicating that Ni in Ni@C exists as metallic particles even through the hydrothermal treatment process.^{29,30} Moreover, the crystallinity of Ni@C/ $Cd_{0.8}Zn_{0.2}S$ is slightly reduced upon enhancing the Ni@C content, implying that the Ni@C can successfully immobilize $Cd_{0.8}Zn_{0.2}S$ nanoparticles and retard the crystal growth.^{32,33}

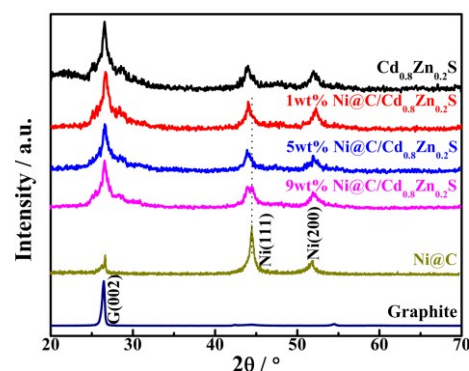


Fig. 1 XRD patterns of the pristine $Cd_{0.8}Zn_{0.2}S$, Ni@C and the Ni@C/ $Cd_{0.8}Zn_{0.2}S$ nanocomposites with different Ni@C contents.

3.2 Microstructure and composition analyses

TEM images in Fig. 2a and b show that 5wt% Ni@C/ $Cd_{0.8}Zn_{0.2}S$ is composed of Ni@C with its graphite-like carbon shells densely decorated by $Cd_{0.8}Zn_{0.2}S$ nanoparticles with an average particle size of ~ 10 nm, whereas Ni@C nanoparticles showing larger particle sizes (~ 50 nm) randomly disperse in the sample, which is similar to our previous report,³⁰ where it is found that the Ni@C nanoparticles have broader size distribution and larger mean particle sizes (~ 40 nm) randomly disperse in the sample. As can be observed from Fig. 2b, the metallic Ni nanoparticle is encapsulated in several carbon layers, the well-resolved lattice fringes with *d*-spacings of *ca.* 0.292, 0.198, and 0.334 nm can be assigned to the $Cd_{0.8}Zn_{0.2}S$ (111), Ni (111), and graphite (002) planes, respectively. It indicated that Ni@C can retain its original structure even after the hydrothermal process. Moreover, those $Cd_{0.8}Zn_{0.2}S$ aggregations are composed of nanoparticles with particle size of ~ 10 nm as shown in Fig. 2c, and the well-resolved lattice fringes with *d*-spacing of ~ 0.292 nm can be ascribed to the (111) planes of $Cd_{0.8}Zn_{0.2}S$, also indicating those $Cd_{0.8}Zn_{0.2}S$ nanoparticles have high crystallinity.

The energy-dispersive X-ray (EDX) spectrum (upper part in Fig. 2d) reveals that the large nanoparticle in Fig. 2b mainly contains Ni and C elements, implying those nanoparticles with larger particle sizes and lower transmissivity in Fig. 2a can be identified as Ni@C nanoparticles, their particle size distribution

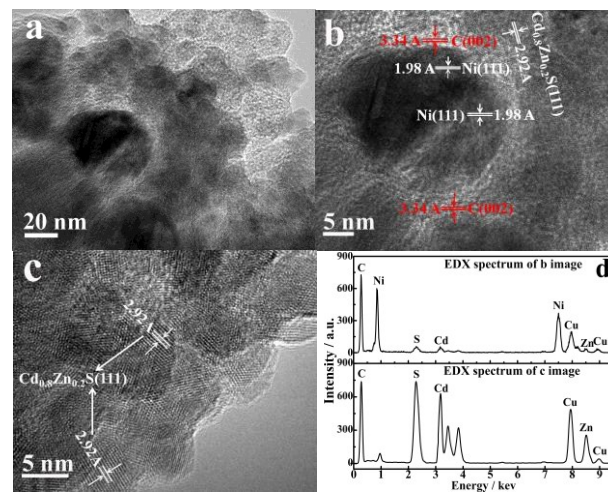


Fig. 2 TEM (a) and HRTEM (b, c) images and EDX spectra (d) of the 5wt% Ni@C/ $Cd_{0.8}Zn_{0.2}S$ nanocomposite.

and morphology are also similar to those of the as-prepared Ni@C.³¹ Where the EDX spectrum (bottom part in Fig. 2d) reveals that those small nanoparticle aggregations mainly contains Cd, Zn and S elements with atom ratio of *ca.* 0.76:0.2:1, implying those nanoparticles with small particle sizes in Fig. 2a and b can be identified as the Cd_{0.8}Zn_{0.2}S nanoparticles.

The surface elemental compositions of the pristine Cd_{0.8}Zn_{0.2}S and 5wt% Ni@C/Cd_{0.8}Zn_{0.2}S were analyzed by XPS spectra (Fig. 3). The survey spectra in Fig. 3a indicate that both of the two products contain Cd, Zn and S elements, and the main binding energy peaks located at 410.9 eV (Cd²⁺ 3d_{5/2}), 404.0 eV (Cd²⁺ 3d_{3/2}), 1042.2 eV (Zn²⁺ 2p_{1/2}), 1019.2 eV (Zn²⁺ 2p_{3/2}), and 161.6 eV (S²⁻ 2p_{3/2}) can be observed from the high resolution XPS spectra (Fig. 3b-d) of the pristine Cd_{0.8}Zn_{0.2}S.³² These binding energy peaks of Cd²⁺ and Zn²⁺ are consistent with the reported data of the CdS-ZnS solid solution with finite deviations.^{4,18,32} After loading with 5wt% Ni@C, slight shifts toward higher binding energies with small intensity decreases can be observed from the high resolution XPS spectra (Fig. 3b-d) of 5wt% Ni@C/Cd_{0.8}Zn_{0.2}S, implying that the binding energies of the core level electrons of those metal and sulphide ions are affected due to the possible interactions among the composite components. No obvious XPS peak ascribable to Ni species can be observed in the range of 845-865 eV binding energy for the 5wt% Ni@C/Cd_{0.8}Zn_{0.2}S, implying that most of Ni species are enveloped by

the graphite-like carbon layers, which is consistent with our previous observation.^{29,30} In addition, the pristine Cd_{0.8}Zn_{0.2}S shows a C 1s peak at 284.1 eV (Fig. 3e), which can be assigned to adventitious carbon. After loading with 5wt% Ni@C, the C 1s peak shifts toward higher binding energy with a broader and stronger asymmetrical peak as shown in the high resolution C 1s spectrum of 5wt% Ni@C/Cd_{0.8}Zn_{0.2}S, implying the coexistence of adventitious carbon and graphite-like carbon in Ni@C.

To further validate this issue, X-ray fluorescence (XRF) analysis results are listed in Table 1. The pristine Cd_{0.8}Zn_{0.2}S has Cd:Zn:S atom ratio of *ca.* 0.77:0.19:1, approximately equals to theoretical stoichiometric ratio of Cd_{0.8}Zn_{0.2}S. Moreover, all Ni@C/Cd_{0.8}Zn_{0.2}S nanocomposites with different Ni@C contents have a Cd:Zn:S atom ratio similar to the pristine Cd_{0.8}Zn_{0.2}S as shown in Table 1, implying the addition of Ni@C has limited influence on the chemical composition of the present ZnS-CdS solid solution. To check the effect of the hydrothermal process on the chemical composition of Ni@C, Ni@C was treated by the same hydrothermal process without addition of the reactants, and the corresponding XRF analysis results are also listed in Table 1. As can be seen, the Ni and C contents in the Ni@C samples with/without hydrothermal treatment are very similar. The pristine Ni@C has Ni:C atom ratio of 0.50:1, while the Ni:C atom ratio in 1wt%, 5wt%, and 9wt% Ni@C/Cd_{0.8}Zn_{0.2}S are 0.48:1, 0.46:1, 0.43:1, respectively. It indicates that the Ni content in

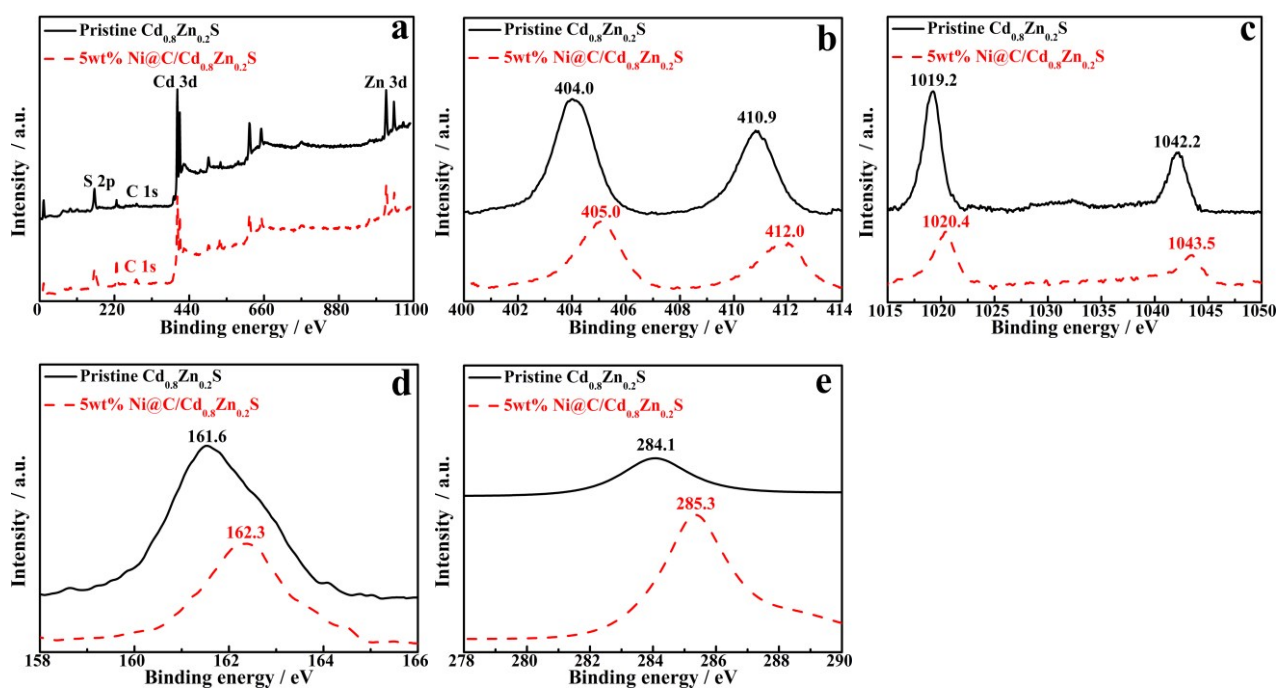


Fig. 3 XPS spectra of the pristine Cd_{0.8}Zn_{0.2}S and the 5wt% Ni@C/Cd_{0.8}Zn_{0.2}S nanocomposite. Survey (a), Cd 3d (b), Zn 3d (c), S 2p (d) and C 1s (e).

Table 1 Element compositions of Ni@C/Cd_{0.8}Zn_{0.2}S containing different Ni@C contents detected by XRF spectrometer

Sample	Pristine Cd _{0.8} Zn _{0.2} S	1wt% Ni@C/ Cd _{0.8} Zn _{0.2} S	5wt% Ni@C/ Cd _{0.8} Zn _{0.2} S	9wt% Ni@C/ Cd _{0.8} Zn _{0.2} S	Pristine Ni@C ^a
C /wt%	—	0.29	1.53	2.80	27.92 (29.15)
Ni /wt%	—	0.68	3.45	5.85	67.54 (67.03)
Cd /wt%	65.71	63.83	62.97	59.45	—
Zn /wt%	9.56	9.04	8.67	8.00	—
S /wt%	24.65	23.71	22.75	21.57	—
Cd:Zn:S atom ratio	0.77:0.19:1	0.77:0.18:1	0.79:0.18:1	0.78:0.18:1	—

^a Data in parentheses are the measured values of Ni@C treated by the same hydrothermal process as Ni@C/Cd_{0.8}Zn_{0.2}S.

Cite this: *Phys. Chem. Chem. Phys.*, 2015, XX,

www.rsc.org/xxxxxx

PAPER

various nanocomposites is slightly lower than its additive content. Moreover, Ni@C content in 1wt%, 5wt%, and 9wt% Ni@C/Cd_{0.8}Zn_{0.2}S is 0.97wt%, 4.98wt%, and 8.65wt%, which is approximate to the corresponding initial addition amount. The above results suggested that the Ni@C nanoparticles have high chemical and thermal stability with very finite loss during the present hydrothermal process.

3.3 Absorption spectra analyses

Fig. 4 shows the UV–Vis diffuse reflectance absorption spectra (DRS) of the pristine Cd_{0.8}Zn_{0.2}S and 5wt% Ni@C/Cd_{0.8}Zn_{0.2}S nanocomposites with different Ni@C contents. The pristine Ni@C exhibits a very broad spectral absorption in the detected wavelength range, and the pristine Cd_{0.8}Zn_{0.2}S shows an absorption edge at *ca.* 555 nm, and its bandgap energy can be estimated to be ~2.23 eV by a related curve of $(\text{d}h\nu)^{1/2}$ vs. photon energy. This bandgap energy is lower than the previously reported value (~2.34 eV) of CdS,^{34,35} but larger than that (~2.16 eV) of the CdS derived from a solvothermal process.⁴ This may be ascribed to the different preparation processes, which might cause the differences in the physical properties such as morphology, particle size, aggregation state, surface states and defects.³⁴⁻³⁶ Although Cd_{0.8}Zn_{0.2}S has no absorption above its fundamental absorption edge rising at ~600 nm, Ni@C/Cd_{0.8}Zn_{0.2}S nanocomposites show a broad elevated background in the visible light region due to the presence of Ni@C. Moreover, the absorbance in the range of 550-700 nm increases with enhancing the Ni@C content in the nanocomposites. It could be attributed to the enhancement of the surface electric charge of the Cd_{0.8}Zn_{0.2}S in the nanocomposite because of the introduction of Ni@C, which leads to the possible electronic transition of $\pi \rightarrow \pi^*$ of Ni@C and $n \rightarrow \pi^*$ between the *n*-orbit of the sulfur species in Cd_{0.8}Zn_{0.2}S and Ni@C.⁴ This enhancement happens at wavelength >550 nm, indicating a more efficient utilization of the solar energy can be obtained. Therefore, it can be inferred that incorporating Ni@C in Cd_{0.8}Zn_{0.2}S particles would influence the photogenerated carrier formation and separation during the photocatalytic process.^{29,30}

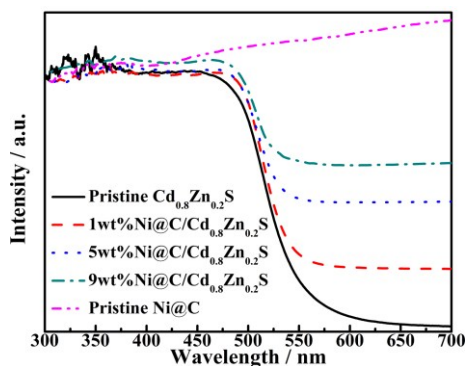


Fig. 4 DRS spectra of the pristine Cd_{0.8}Zn_{0.2}S, Ni@C, and the Ni@C/Cd_{0.8}Zn_{0.2}S nanocomposites with different Ni@C contents.

3.4 Photocatalytic H₂ production activity analyses

Photocatalytic H₂ production experiment was conducted by using an aqueous suspension containing photocatalyst (100 mg) and Na₂S (0.25M)-Na₂SO₃ (0.35M) solution under visible-light ($\lambda \geq 420$ nm) irradiation. Preliminary test indicated that no obvious H₂ evolution can be detected in the absence of either photocatalyst or visible-light irradiation. The effects of Ni@C contents in the nanocomposite on the average photocatalytic H₂ production rate under 5 h visible-light irradiation were investigated and shown in Fig. 5. As can be seen, the pristine Ni@C shows very limited activity (20.6 $\mu\text{mol h}^{-1}$) for H₂ production, and the Ni@C treated by the hydrothermal process still exhibits a similar activity (21.3 $\mu\text{mol h}^{-1}$), also implying the present hydrothermal process does not destroy the original structure of Ni@C as mentioned above. Moreover, all Ni@C/Cd_{0.8}Zn_{0.2}S nanocomposites with different Ni@C contents show higher activity than the pristine Cd_{0.8}Zn_{0.2}S. The increased H₂ production activity with enhancing the Ni@C content from 0 to 5wt% could be attributed to the distinctive structure and electrical properties of the Ni@C/Cd_{0.8}Zn_{0.2}S, which is beneficial for the separation of the photogenerated carriers. Since the pristine Ni@C shows very limited activity (20.6 $\mu\text{mol h}^{-1}$), it is reasonable to think that the excessive Ni@C may hinder the nanocomposite's light absorption and lead to the decrease of the Cd_{0.8}Zn_{0.2}S relative content, which would decrease the electrons excited from the valence band (VB) of Cd_{0.8}Zn_{0.2}S. Thus, the activity exhibits a decreasing trend with further enhancing the Ni@C content exceeding 5wt%. As a result, 5wt% Ni@C/Cd_{0.8}Zn_{0.2}S has the maximum mean H₂ production activity (969.5 $\mu\text{mol h}^{-1}$), which is ~3.10 times higher than that (312.6 $\mu\text{mol h}^{-1}$) of the pristine Cd_{0.8}Zn_{0.2}S. Furthermore, the physical mixture (Ni@C+Cd_{0.8}Zn_{0.2}S) containing 5wt% Ni@C and 95wt% Cd_{0.8}Zn_{0.2}S also exhibits higher H₂ production activity (426.7 $\mu\text{mol h}^{-1}$) than that (312.6 $\mu\text{mol h}^{-1}$) of the pristine Cd_{0.8}Zn_{0.2}S although it is much lower than that (969.5 $\mu\text{mol h}^{-1}$) of 5wt% Ni@C/Cd_{0.8}Zn_{0.2}S. This also indicates that incorporating Ni@C can promote the photoactivity of Cd_{0.8}Zn_{0.2}S.

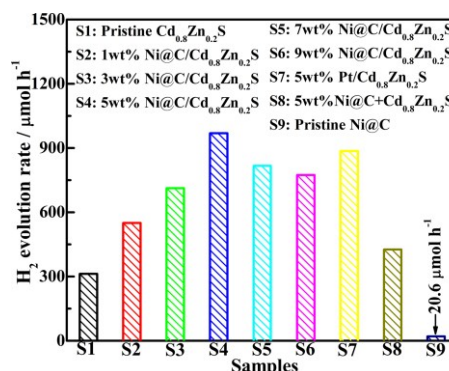


Fig. 5 Photocatalytic H₂ production activities of various products under visible-light irradiation. Conditions: 100 mg photocatalysts in 100 mL Na₂S (0.25M)-Na₂SO₃ (0.35M) solution, 300 W Xe-lamp equipped with cut-off filter ($\lambda \geq 420$ nm) for 5 h light irradiation.

It is well known that Pt nanoparticles as co-catalyst can enhance the photoactivity of metal sulphides.^{32,37,38} In the present study, it is also found that Pt-loading can also significantly enhance the H₂ production activity of Cd_{0.8}Zn_{0.2}S as shown in Fig. 5. 5wt% Pt/Cd_{0.8}Zn_{0.2}S exhibits considerable H₂ production activity (885.9 μmol h⁻¹), which is slightly lower than that (969.5 μmol h⁻¹) of 5wt% Ni@C/Cd_{0.8}Zn_{0.2}S but much higher than that of the pristine Cd_{0.8}Zn_{0.2}S. However, Pt as co-catalyst suffers from the disadvantages of being rare and expensive, which limited their practical application in the photocatalytic H₂ production as mentioned above.²² Moreover, the graphite-like shells of Ni@C would block the accessibility of reaction solution to the metal Ni core, which might suppress the H₂ production reaction and its release to gas phase, and then lead to a reduced activity. As a stable charge carrier, the graphite-like carbon shell is a more efficient electron conductor to transfer its accepted electrons to the metallic Ni core.³⁰ Namely, the carbon shell of Ni@C also acted important role on improving the photoactivity and stability of Cd_{0.8}Zn_{0.2}S. Therefore, it can be concluded that the activity enhancement of the Ni@C/Cd_{0.8}Zn_{0.2}S can be attributed to the synergistic effect among its composite components, where the metallic Ni in Ni@C acted as co-catalyst while the graphite-like carbon shells as Cd_{0.8}Zn_{0.2}S nanoparticles' support and electron acceptor, which is beneficial for separating spatially the photo-generated carriers and improving the photoactivity and stability for H₂ production.³⁰ Moreover, the present findings also demonstrate a cost reduction strategy by using non-noble metal co-catalyst instead of noble ones for efficient and stable light-to-hydrogen energy conversion.

3.5 Photocatalytic H₂ production stability analyses

The above conjecture on the stability can be validated by the time courses (Fig. 6) for the H₂ production of the representative products. The H₂ production amount over those photocatalysts in five runs, in which fresh sacrificial reagents solution periodically is replaced in each run. As can be seen, the 5wt% Ni@C/Cd_{0.8}Zn_{0.2}S can produce more than 23.0 mmol H₂ during 25 h photoreaction with an average H₂ generation rate of 969.5 μmol h⁻¹ in the first run of 5 h photoreaction, and then slightly declines to 953.3, 929.0, 897.2, and 867.7 μmol h⁻¹ in the second, third, fourth and fifth run of 5 h photoreaction, respectively. The percentages of the average H₂ production rate of the second, third, fourth and fifth run as compared to the first run's are estimated to be 98.3%, 95.8%, 92.5%, and 89.5%, respectively. Similarly, 5wt% Pt/Cd_{0.8}Zn_{0.2}S shows a slightly declines in the average H₂ production rate in the 5 runs as shown in Fig. 6. Whereas, the pristine Cd_{0.8}Zn_{0.2}S and the mixture (5wt% Ni@C+Cd_{0.8}Zn_{0.2}S) shows more obvious declines in the average H₂ production rate in the 5 runs. After the five run, the corresponding percentages of the average H₂ production rate as compared to the first run's are calculated to be 51.3% for the pristine Cd_{0.8}Zn_{0.2}S and 76.5% for the 5wt% Ni@C+Cd_{0.8}Zn_{0.2}S, respectively. The above results indicate that the existence of Ni@C can improve both the photoactivity and stability of Cd_{0.8}Zn_{0.2}S.

Atomic absorption spectrum (AAS) analysis results (Fig. 7) of the supernatant of 5wt% Ni@C/Cd_{0.8}Zn_{0.2}S suspension after each 5 h photoreaction process and removal of the photocatalyst shows that no obvious change in the Ni concentration, indicating very finite Ni corrosion occurring during the photoreaction process

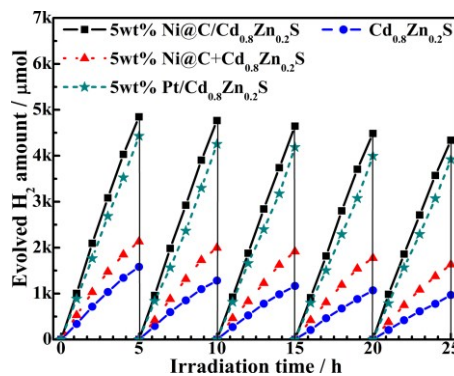


Fig. 6 Typical time course for H₂ production over of various products under visible-light irradiation. Conditions: 100 mg photocatalysts in 100 mL Na₂S (0.25M)-Na₂SO₃ (0.35M) solution, 300 W Xe-lamp equipped with cut-off filter ($\lambda \geq 420$ nm) for 5 h light irradiation.

Moreover, the Cd²⁺ content in the five runs (for each 5 h) photoreaction suspension also verifies the photostability of the metal sulphide solid solution. There is total 6.60 μg mL⁻¹ Cd²⁺ in the remnant solution for the 5wt% Ni@C/Cd_{0.8}Zn_{0.2}S suspension, while the Cd content in the present 100 mL suspension containing 5wt% Ni@C/Cd_{0.8}Zn_{0.2}S (100 mg) is ~632.8 μg mL⁻¹. Namely, only ~1.0wt% Cd in the nanocomposite is released to suspension during the 25 h photoreaction, implying the very limited photocorrosion of Cd_{0.8}Zn_{0.2}S in the present nanocomposite.

To further obtain more firm evidence on this issue, the nanocomposite was replaced by the pristine Cd_{0.8}Zn_{0.2}S for each 5 h photoreaction under the same condition, and the Cd²⁺ content in the remnant solution after removal of Cd_{0.8}Zn_{0.2}S is 34.71 μg mL⁻¹. Namely, the released Cd²⁺ from the pristine Cd_{0.8}Zn_{0.2}S is ~5.2wt% Cd²⁺, much larger than that from the nanocomposites. This is similar to the previous reports that the presence of multiwalled carbon nanotubes (MWCNTs) can hamper the photocorrosion of sulphide solid solution and therefore improve its photostability.^{39,40} Thus, it can be concluded that the incorporation of Ni@C can efficiently enhance the photo-stability of Cd_{0.8}Zn_{0.2}S, and the present carbon encapsulation strategy of Ni co-catalyst exerted important role in the present photocatalytic system with high efficiency and good chemical/thermal stability.

3.6 Discussion on the photocatalytic mechanism

Fig. 8 depicts the apparent quantum yield (AQY) curves and the DRS spectrum of the 5wt% Ni@C/Cd_{0.8}Zn_{0.2}S. As can be seen,

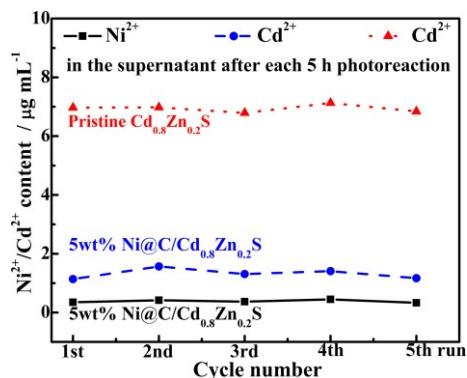


Fig. 7 Ni²⁺/Cd²⁺ contents in the supernatant of the pristine Cd_{0.8}Zn_{0.2}S and the 5wt% Ni@C/Cd_{0.8}Zn_{0.2}S suspension after each 5 h photoreaction.

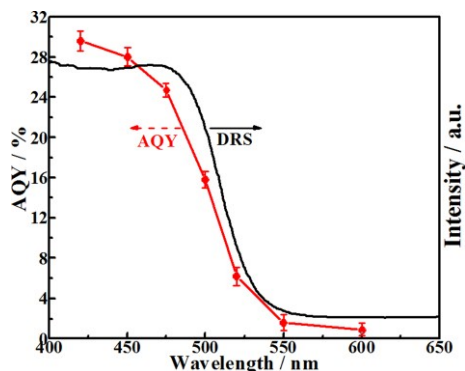


Fig. 8 Comparison of AQY curves and DRS spectrum of 5wt% Ni@C/Cd_{0.8}Zn_{0.2}S. The light intensity of monochromatic wavelengths through 420, 450, 475, 500, 520, and 550 nm band pass filters is 8.5, 8.2, 14.3, 13.0, 13.2, and 13.2 mW/cm², respectively.

5wt% Ni@C/Cd_{0.8}Zn_{0.2}S shows a spectral responsive wavelengths ranging from 420 to 600 nm, and the AQY value at 420, 450, 475, 500, 520, 550, and 600 nm monochromatic light irradiation is *ca.* 29.6%, 28.0%, 24.7%, 15.8%, 6.2%, 1.6%, and 0.9%, respectively. When the wavelength is longer than 600 nm, 5wt% Ni@C/Cd_{0.8}Zn_{0.2}S shows no obvious H₂ production. Obviously, the AQY value decreases with enhancing the incident light wavelength, and the wavelengths suitable for H₂ evolution are basically coincided with the absorption edge of Cd_{0.8}Zn_{0.2}S even though those nanocomposites still shows high absorbance at wavelength larger than 600 nm, indicating that the H₂ evolution reaction was indeed driven by the photoinduced Cd_{0.8}Zn_{0.2}S excitation, and the light absorption property of Cd_{0.8}Zn_{0.2}S in the nanocomposite governed the photoactivity for H₂ production.^{41,42}

Considering our results and discussion in the photoactivity and stability sections, a possible mechanism for H₂ production over Ni@C/Cd_{0.8}Zn_{0.2}S can be proposed as follows: The primary role of Ni@C in Cd_{0.8}Zn_{0.2}S photoreaction is possibly to be the CB electron acceptor since the graphite carbon has a more positively leveled work function (*ca.* 4.60 eV⁴¹) compared to the CB level (*ca.* 3.49 eV^{13,35}) of Cd_{0.8}Zn_{0.2}S. It indicates that the charge transfer from Cd_{0.8}Zn_{0.2}S to carbon shell of Ni@C is thermodynamically favorable, which is similar to the previous situation that the charge transfer from photo-excited CdS to the MWCNTs.¹³ Thus, a similar charge transfer mechanism can be used to the present Ni@C/Cd_{0.8}Zn_{0.2}S system. Since the graphite carbon shells of Ni@C nanoparticles have a more positively leveled work function than Cd_{0.8}Zn_{0.2}S as discussed above,^{13,35,43} the VB electrons of Cd_{0.8}Zn_{0.2}S can be excited to its CB, and then transfer to the densely contacted carbon shell of Ni@C, where those electrons can further accumulate on Ni nanoparticles, and then react with the adsorbed proton/water to produce H₂.^{21,32} In addition, the graphite-like carbon as the supporting matrix of Cd_{0.8}Zn_{0.2}S nanoparticles can transfer those electrons from Cd_{0.8}Zn_{0.2}S quickly, and resulting in the suppression of the carrier recombination.^{30,38} Moreover, the work function (*ca.* 4.60 eV) of carbon shell is greater than the CB energy level (*ca.* 3.49 eV) of Cd_{0.8}Zn_{0.2}S, but is smaller than that (*ca.* 5.35 eV) of metal Ni cocatalyst,^{13,43} which also causing to a facile charge transfer from carbon shell to Ni and resulting in high H₂ production activity. Therefore, it is reasonable to think that the synergy effect is the crucial for the efficient electron transfer and separation, and then

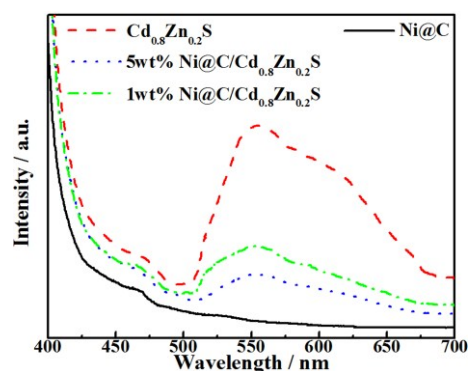


Fig. 9 PL spectra of the pristine Cd_{0.8}Zn_{0.2}S, the Ni@C/Cd_{0.8}Zn_{0.2}S nanocomposites with 1wt% and 5wt% Ni@C contents under an excitation wavelength of 380 nm.

for the significant enhancement in the photoactivity. Of course, the above mentioned relative energetics is just one of many factors that influences the charge transfer processes of the photoreaction system, and the other influencing factors such as proton adsorption/desorption energy, intrinsic rates of electron transfer (e.g., exchange current), and particle size effects etc, seem to influence H₂ production with different extents.¹³

The above assumption on the charge transfer trend can be further validated by the photoluminescence (PL) spectra shown in Fig. 9. As can be seen, the pristine Cd_{0.8}Zn_{0.2}S nanoparticles exhibits a strong broad peak locates at *ca.* 555 nm, which can be ascribed to the bandgap excitation of Cd_{0.8}Zn_{0.2}S.^{22,32} A significant PL quenching of Cd_{0.8}Zn_{0.2}S can be observed after coupling with 1wt% or 5wt% Ni@C though the pristine Ni@C shows no obvious emission as shown in Fig. 9. Namely, the fluorescence quenching effect is mainly due to the addition of Ni@C though Ni and C species may hinder light absorption by Cd_{0.8}Zn_{0.2}S more or less. This result indicates the photogenerated carriers in Cd_{0.8}Zn_{0.2}S can be effectively transfer towards the densely contacted carbon shells of the Ni@C, and then to Ni for H₂ production.³² The better charge separation and spectral resonance of the present nanocomposites can also be observed from the photocurrent responses (*J-V* curves) of the suspension consisting of photocatalysts shown in Fig. 10. The stable photocurrent value of 5wt% Ni@C/Cd_{0.8}Zn_{0.2}S nanocomposite is ~3.12 times higher than that of the pristine Cd_{0.8}Zn_{0.2}S. It can be ascribed to the synergetic effect existing in the Ni@C/Cd_{0.8}Zn_{0.2}S interface, where the photogenerated charge can be efficiently separated in space to lower the carrier recombination.

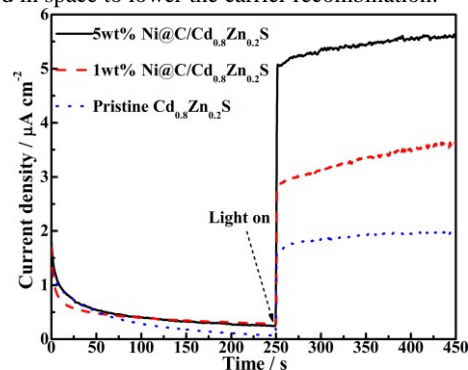


Fig. 10 Photocurrent-time curves of the pristine Cd_{0.8}Zn_{0.2}S, the Ni@C/Cd_{0.8}Zn_{0.2}S nanocomposites with 1wt% and 5wt% Ni@C contents in NaOH solution under visible-light irradiation.

Apparently, the graphite-like carbon coating on metal Ni nanoparticles acted not only as protection layers of the Ni core and supporting matrix of the Cd_{0.8}Zn_{0.2}S nanoparticles, but also as electron acceptor to increase the electron acceptance and transport rates in the nanocomposite, and then the photogenerated carriers recombination can be efficiently suppressed, this phenomena might be also beneficial for the photocatalytic reactions.³⁰ The above results suggested interesting possibility for the fabrication of carbon encapsulated Ni co-catalyst coupled in metal sulphide photocatalysts, which is helpful to hinder the backward electron transfer and improve the electron injection and quantum efficiency. Anyway, the present Ni co-catalyst encapsulation is a successful cost reduction strategy by using non-noble metal co-catalyst instead of noble ones for efficient and stable light-to-hydrogen energy conversion.

4. Conclusions

Carbon encapsulation strategy of Ni co-catalyst is applied to the fabrication of novel carbon-coated Ni (Ni@C)/Cd_{0.8}Zn_{0.2}S nanocomposites derived from a facile hydrothermal process by using a pre-prepared Ni@C as a starting material. The obtained Ni@C/Cd_{0.8}Zn_{0.2}S exhibit much better photoactivity and stability for H₂ production than the pristine Cd_{0.8}Zn_{0.2}S, and 5wt% Ni@C/Cd_{0.8}Zn_{0.2}S exhibits the maximum average photocatalytic H₂ production activity (969.5 μmol h⁻¹) and an apparent quantum yield up to ca. 29.6% under 420 nm monochromatic light irradiation. The metallic Ni in Ni@C acted as co-catalyst while the graphite-like carbon as Cd_{0.8}Zn_{0.2}S nanoparticles' support and electron acceptor, which causing an efficient charge separation, and then the enhanced photoactivity and stability for H₂ production as compared to the pristine Cd_{0.8}Zn_{0.2}S. The present results suggested interesting possibility for the fabrication of carbon encapsulated Ni co-catalyst coupled in metal sulphide photocatalysts, and demonstrates an effective cost reduction strategy by using non-noble metal co-catalyst instead of noble ones for cheap, efficient and steady H₂ production system.

Acknowledgments

The present work is supported by the Natural Science Foundation of China (21271146, 20973128, and 20871096), the Funds for Creative Research Groups of Hubei Province (2014CFA007), and the Fundamental Research Funds for the Central Universities (2042014kf0228), China.

References

- 1 A. Fujishima and K. Honda, *Nature*, 1972, **238**, 37-38.
- 2 H. Wang, L. Zhang, Z. Chen, J. Hu, S. Li, Z. Wang, J. Liu and X. Wang, *Chem. Soc. Rev.*, 2014, **43**, 5234-5244.
- 3 C. Wang, J. Hu, C. Wu, H. Kuo, Y. Chang, Z. Lan, H. Wu, E. Diau and C. Lin, *Energy Environ. Sci.*, 2014, **7**, 1392-1396.
- 4 X. J. Liu, P. Zeng, T. Y. Peng, X. H. Zhang and K. J. Deng, *Int. J. Hydrogen Energy*, 2012, **37**, 1375-1384.
- 5 X. H. Zhang, L. J. Yu, C. S. Zhuang, T. Y. Peng, R. J. Li and X. G. Li, *ACS Catal.*, 2014, **4**, 162-170.
- 6 X. H. Zhang, U. Veikko, J. Mao, P. Cai and T. Y. Peng, *Chem. Eur. J.*, 2012, **18**, 12103-12111.
- 7 K. Li, B. Chai, T. Y. Peng, J. Mao and L. Zan, *ACS Catal.*, 2013, **3**, 170-177.
- 8 M. Matsumura, Y. Saho and H. Tsubomura, *J. Phys. Chem.*, 1983, **87**, 3807-3808.
- 9 J. F. Reber and M. Rusek, *J. Phys. Chem.*, 1986, **90**, 824-834.
- 10 Y. X. Li, Y. F. Hu, S. Q. Peng, G. X. Lu and S. B. Li, *J. Phys. Chem. C*, 2009, **113**, 9352-9358.
- 11 D. Meissner, R. Memming, B. Kastening, *J. Phys. Chem.*, 1988, **92**, 3476-3483.
- 12 Q. Li, B. D. Guo, J. G. Yu, J. R. Ran, B. H. Zhang, H. J. Yan, J. R. Gong, *J. Am. Chem. Soc.*, 2011, **133**, 10878-10884.
- 13 Y. K. Kim and H. Park, *Energy Environ. Sci.*, 2011, **4**, 685-694.
- 14 T. A. Pham, B. C. Choi and Y. T. Jeong, *Nanotechnology*, 2010, **21**, 465603.
- 15 K. Zhang, D. W. Jing, C. J. Xing and L. J. Guo, *Int. J. Hydrogen Energy*, 2007, **32**, 4685-4691.
- 16 K. Zhang, D. W. Jing, Q. Y. Chen and L. J. Guo, *Int. J. Hydrogen Energy*, 2010, **35**, 2048-2057.
- 17 Y. X. Li, D. Gao, S. Q. Peng, G. X. Lu and S. B. Li, *Int. J. Hydrogen Energy*, 2011, **36**, 4291-4297.
- 18 W. Zhang and R. Xu, *Int. J. Hydrogen Energy*, 2009, **34**, 8495-8503.
- 19 C. J. Xing, Y. J. Zhang, W. Yan and L. J. Guo, *Int. J. Hydrogen Energy*, 2006, **31**, 2018-2024.
- 20 P. Fornasiero, V. Gombac, L. Sordelli, T. Montini, J. J. Delgado, A. Adamski, G. Adami, M. Cargnello and S. Bernal, *J. Phys. Chem. A*, 2010, **114**, 3916-3925.
- 21 C. C. Hu and H. S. Teng, *J. Catal.*, 2010, **272**, 1-8.
- 22 K. Shimizu, S. Itoh, T. Hatamachi, T. Kodama, M. Sato and K. Toda, *Chem. Mater.*, 2005, **17**, 5161-5166.
- 23 H. Yan, J. Yang, G. Ma, G. Wu, X. Zong, Z. Lei, J. Shi and C. Li, *J. Catal.*, 2009, **266**, 165-168.
- 24 P. Gao, J. C. Liu, S. Lee, T. Zhang and D. D. Sun, *J. Mater. Chem.*, 2010, **22**, 2292-2298.
- 25 Y. X. Li, S. Y. Lin, S. Q. Peng, G. X. Lu and S. B. Li, *Int. J. Hydrogen Energy*, 2013, **38**, 15976-15984.
- 26 F. Schuth, A. H. Lu and E. L. Salabas, *Angew. Chem. Int. Ed.*, 2007, **46**, 1222-1244.
- 27 X. G. Liu, B. Li, D. Y. Geng, W. B. Cui, F. Yang, Z. G. Xie, D. J. Kang and Z. D. Zhang, *Carbon*, 2009, **47**, 470-474.
- 28 K. Maeda, N. Sakamoto, T. Ikeda, H. Ohtsuka, A. Xiong, D. Lu, M. Kanehara, T. Teranishi and K. Domen, *Chem. Eur. J.*, 2010, **16**, 7750-7759.
- 29 P. Zeng, X. G. Zhang, X. H. Zhang, B. Chai and T. Y. Peng, *Chem. Phys. Lett.*, 2011, **503**, 262-265.
- 30 T. Y. Peng, X. H. Zhang, P. Zeng, K. Li, X. G. Zhang and X. G. Li, *J. Catal.*, 2013, **303**, 156-163.
- 31 J. Ling, Y. Liu, G. M. Hao and X. G. Zhang, *Mater. Sci. Eng. B*, 2003, **100**, 186-190.
- 32 P. Wang, T. F. Jiang, C. Z. Zhu, Y. M. Zhai, D. J. Wang and S. J. Dong, *Nano Res*, 2010, **3**, 794-799.
- 33 T. Y. Peng, K. Li, P. Zeng, Q. G. Zhang and X. G. Zhang, *J. Phys. Chem. C*, 2012, **116**, 22720-22726.
- 34 T. R. Ravindran, A. K. Arora, B. Balamurugan and B. R. Mehta, *Nanostruct. Mater.*, 1999, **11**, 603-609.
- 35 P. Zeng, Q. G. Zhang, T. Y. Peng and X. H. Zhang, *Phys. Chem. Chem. Phys.*, 2011, **13**, 21496-21502.
- 36 W. O. Milligan, *J. Phys. Chem.*, 1934, **38**, 797-803.
- 37 S. Dag and L. W. Wang, *Phys. Rev. B*, 2010, **82**, 241303-241305.
- 38 Y. Miseki, H. Kato and A. Kudo, *Chem. Lett.*, 2005, **34**, 54-56.
- 39 L. L. Ma, H. Z. Sun, Y. G. Zhang, Y. L. Lin, J. L. Li, E. K. Wang, Y. Yu, M. Tan and J. B. Wang, *Nanotechnology*, 2008, **19**, 115709.
- 40 J. Cao, J. Z. Sun, J. Hong, H. Y. Li, H. Z. Chen and M. Wang, *Adv. Mater.*, 2004, **16**, 84-87.
- 41 O. M. Wilson, R. W. J. Scott, J. C. Garcia-Martinez and R. M. Crooks, *J. Am. Chem. Soc.*, 2005, **127**, 1015-1024.
- 42 V. Kolkovskiy, L. Dobaczewski, K. B. Nielsen, V. Kolkovskiy, A. N. Larsen and J. Weber, *Phys. B*, 2009, **404**, 5080-5084.
- 43 S. Suzuki, C. Bower, Y. Watanabe and O. Zhou, *Appl. Phys. Lett.*, 2000, **76**, 4007-4009.